JOURNAL OF AIRCRAFT
Vol. 37, No. 6, November–December 2000

Study of High-Lift Configurations Using k–ζ Transition/Turbulence Model

Ryan Czerwiec* and J. R. Edwards†
North Carolina State University, Raleigh, North Carolina 27695-7910
C. L. Rumsey‡
NASA Langley Research Center, Hampton, Virginia 23681-2199
A. Bertelrud§
Analytical Services and Materials, Inc., Hampton, Virginia 23666
and
H. A. Hassan¶
North Carolina State University, Raleigh, North Carolina 27695-7910

The flow over the multi-element McDonnell Douglas configuration is computed using the k–ζ transition/turbulence model. The model is capable of calculating transition onset as part of the solution at a cost comparable to Navier–Stokes solvers that employ two-equation models. The model is first incorporated into CFL3D and then used to calculate flows for two angles of attack, 8 and 19 deg, at a freestream Mach number of 0.2 and a Reynolds number of 9×10^6. In general, good agreement is indicated for predicting transition onset and velocity profiles over sections of the main airfoil and flap. Most of the differences between computation and experiment are in the prediction of the extent and penetration of the slat wake at the 19-deg angle-of-attack case. Even for this case relative differences were less than 5%.

Introduction

THE prediction of flows past high-lift configuration is an extremely difficult problem that proved to be a challenge to existing computational fluid dynamics (CFD) codes. High-lift flows are characterized by confluent boundary layers in which multiple shear layers interact. Thus, significant interaction takes place between the slat wake and the boundary layer on the main airfoil and confluent boundary layer on the main airfoil and flap. These complex interactions result in a flowfield that is capable of tolerating high adverse pressure gradients without separation.

The inability of widely used Reynolds-averaged Navier–Stokes solvers[1–3] to predict high-lift flows can be traced to two important limitations. The first is the absence of models capable of predicting the onset and extent of transition. Methods based on the e^n method or the parabolic stability equation (PSE) have yet to be integrated into Navier–Stokes solvers.[4] Calculation of transition onset using such codes requires many inputs, many different codes, and an experienced person. Even when such onset is calculated, the interactive nature of the calculation requires an incredible amount of computer resources. As a result, the closest thing to coupling the e^n method to existing Navier–Stokes solvers[5,6] is the use of the approximate integral method of Drela and Giles.[7] In addition to the preceding, e^n methods or methods based on the PSE cannot provide any information on the extent of transition.

The second limitation of existing codes is the inadequacy of the turbulence models employed. As shown by Wilcox,[8] the majority of the widely used turbulence models cannot do an adequate job calculating wall-bounded shear flows without sacrificing performance when calculating free shear layers. Thus, one major limitation of existing codes is their inability to calculate wake flows emanating from the slat, main element, and flaps, and their interaction with the boundary-layer flow in an accurate manner. This shortcoming may be linked to an inadequate length-scale equation.[9] A related limitation is in the calculation of nonturbulent flows. Current procedures require zeroing out production terms in the turbulent equations prior to the specified transition point. The resulting equations are not suited to calculate the flow response in the transitional region.

Bertelrud[10] has undertaken a thorough evaluation of existing transition prediction methods for high-lift devices. He concluded that none of the published criteria appear to provide predictive capability for such flows. This is to be expected because these methods were not designed for confluent boundary layers.

The object of this investigation is to implement the recently developed k–ζ transition/turbulence model[11] into CFL3D and to use the resulting code to study flows past multielement airfoils. The model of Ref. 11 does not suffer from the limitations just presented. Once the transition mechanism and criteria are identified, the model predicts the onset and extent of transition and the rest of the flowfield without having to utilize stability or boundary-layer codes.

CFL3D has been one of the most widely used codes in the calculation of multielement airfoils in takeoff and landing configurations. A number of investigators have used the code to calculate some of the test conditions from the extensive experimental database that has been generated. Pressure distributions, velocity distributions, Reynolds stresses, and the onset and extent of transition regions have been documented for a wide range of angles of attack and Reynolds numbers.[12–16] The database exhibits a variety of physical phenomena, which vary depending on the angle of attack.

Formulation of the Problem

Approach

The model being implemented in CFL3D is based on a recently developed transition/turbulence model.[11] In this approach the nonturbulent fluctuations in a fluid are treated in a manner similar to that used in describing turbulence. The turbulent part of the model is based on the recently developed k–ζ (enstrophy) model.[17]

Received 11 May 1999; presented as Paper 99-3186 at the AIAA 17th Applied Aerodynamics Conference, Norfolk, VA, 28 June–1 July 1999; revision received 10 April 2000; accepted for publication 14 April 2000.

*Research Assistant, Mechanical and Aerospace Engineering, Box 7910.
†Assistant Professor, Mechanical and Aerospace Engineering, Box 7910.
‡Senior Research Scientist, Fluid Mechanics and Acoustics Division.
§Senior Scientist.
¶Professor, Mechanical and Aerospace Engineering, Box 7910.

What distinguishes the k–ζ model from other models is that the length-scale equation is based on the exact enstrophy (variance of vorticity) equation, which can be derived from the Navier–Stokes equations, and not on an empirical model equation. Thus, the model takes into consideration the relevant physics of the flow.

Because this turbulence model is a two-equation model, the transition/turbulence model makes use of an eddy viscosity approach for the nonturbulent fluctuations. The eddy viscosity for the nonturbulent part of the flow is deduced from results of linear stability theory.[18] This is accomplished in most cases by determining the frequency of the mode with the maximum amplification rate.

Traditionally, the transition problem has been treated as a combination of two problems. The first deals with the transition extent, given the onset, whereas the second deals with the transition onset. One of the methods employed in calculating the extent is to replace the turbulent viscosity by

$$\Gamma \mu_t \tag{1}$$

where μ_t is the turbulent viscosity and Γ is the intermittency, or the fraction of the time the flow is turbulent at a given location. Γ varies from 0, at onset, to 1, when the transition to turbulence is complete. The most widely used expression for Γ is that of Dhawan and Narasimha.[19] There are many ways that are being used to specify transition onset: selection based on experiment, experimental correlation, or use of stability theory. Methods based on stability theory employ the e^n method or a method based on the PSE.

Even when the transition onset is specified from results of an experiment, Eq. (1) does not perform well. One of the reasons for this behavior is because the preceding formula does not account for the nonturbulent fluctuations that eventually lead to transition. As a result, the present model replaces μ_t by

$$(1 - \Gamma)\mu_{\mathrm{nt}} + \Gamma \mu_t \tag{2}$$

where μ_{nt} represents the contribution of the nonturbulent fluctuations. In the present work an expression for μ_{nt} was derived using results from linear stability theory.

In the present model the constitutive stress-strain relations for the nonturbulent fluctuations are derived from observed or computed characteristics of Tollmien–Schlichting (T–S) waves. The eddy viscosity μ_{nt} is set as

$$\mu_{\mathrm{nt}} = C_\mu \rho k \tau, \qquad C_\mu = 0.09 \tag{3}$$

where k is the fluctuation kinetic energy per unit mass, ρ is the density, and τ is a timescale characteristic of the type of the instability being considered. Although the present approach makes no direct use of stability codes, expressions for τ were modeled using results obtained from linear stability theory.

The turbulence model is based on the k–ζ model of Robinson and Hassan.[17] This model is free of damping and wall functions and is coordinate independent. Furthermore, all modeled correlations are tensorially consistent and Galilean invariant. It reproduces the correct growth rates of all free shear layers and is capable of predicting separated flow in the presence and absence of shocks. It incorporates relevant compressibility effects and has been demonstrated for both two- and three-dimensional separated flows where Morkovin's hypothesis is expected to hold. Thus, the model should be capable of calculating multielement airfoils at various angles of attack and Reynolds numbers.

For transition resulting from T–S waves,[18]

$$\tau = a/\omega \tag{4}$$

where a is a model constant that depends on the freestream turbulence intensity Tu, defined as

$$Tu = 100\sqrt{\tfrac{2}{3}\left(k_\infty \mid q_\infty^2\right)} \tag{5}$$

where k_∞ and q_∞ are the freestream kinetic energy of the fluctuations and magnitude of freestream velocity. The model constant has the form

$$a = 0.095(Tu - 0.138)^2 + 0.01122 \tag{6}$$

The quantity ω is the frequency of the first mode disturbance having the maximum amplification rate.

References 11 and 18 present an expression for ω, which requires calculation of the displacement thickness. Because CFL3D has no provision for calculating boundary-layer quantities, a new correlation, derived from Fig. 6.13 of Ref. 20, is used. This correlation can be expressed as

$$\omega\nu \mid q_e^2 = 0.48 Re_x^{-0.65} \tag{7}$$

where q_e is the edge velocity, ν is the kinematic viscosity, and Re_x is the Reynolds number based on a distance measured from the stagnation point. The edge velocity is calculated from the assumption that the pressure normal to the surface is constant within the boundary layer. This assumption is not quite accurate for confluent boundary layers. However, as is seen next, the slight inaccuracy in calculating the edge velocity has a minimal effect on the results. The quantity a in Eq. (6) is 1.38 times the value in Ref. 11. This is needed to account for the differences between Eq. (7) and Walker's correlation,[21] which involves a displacement thickness.

As is seen from Eq. (7), ω depends on the Reynolds number and edge velocity. Thus, it accounts for both Reynolds number and pressure gradient effects. When this is coupled with Eqs. (3) and (4), one can see that the transition mechanism is influenced by freestream turbulence intensity, pressure gradient, and Reynolds number—the three factors that were deemed relevant by Bertelrud[9] in his study of transition on high-lift devices.

Intermittency

The Dhawan and Narasimha expression is given by

$$\Gamma = 1 - \exp(-0.412\xi^2) \tag{8}$$

with

$$\xi = \max(x - x_t, 0)/\lambda \tag{9}$$

where λ is a characteristic extent of the transitional region. An experimental correlation between λ and x_t is

$$Re_\lambda = 9.0 Re_{x_t}^{0.75} \tag{10}$$

with x_t being the location where turbulent spots first appear or where skin friction is a minimum. In this work this is determined as part of the solution. Thus, using the preceding approach the user does not have to specify either the onset or extent of transition. Moreover, the preceding approach can be incorporated into any existing CFD code with the resulting run time being slightly more than a typical code that incorporates a two-equation turbulence model.

Experimental and Computational Transition Criteria

Characteristics of hot films were used to infer transition for the high-lift configurations under consideration.[15] Three measurements were used to infer transition: standard deviation, skewness, and flatness of the hot-film signal. The three measurements gave different transitional regions, and the selected onset and extent involved some subjective judgment. Figure 1, which is taken from Ref. 15, illustrates the preceding point.

The traditional criteria for determining onset of transition are minimum skin friction, minimum heat flux, or minimum recovery factors for adiabatic walls. In principle, these criteria can be inferred from hot-film data. This, however, is not available at present. Two-equation models do not calculate skewness or flatness, whereas the

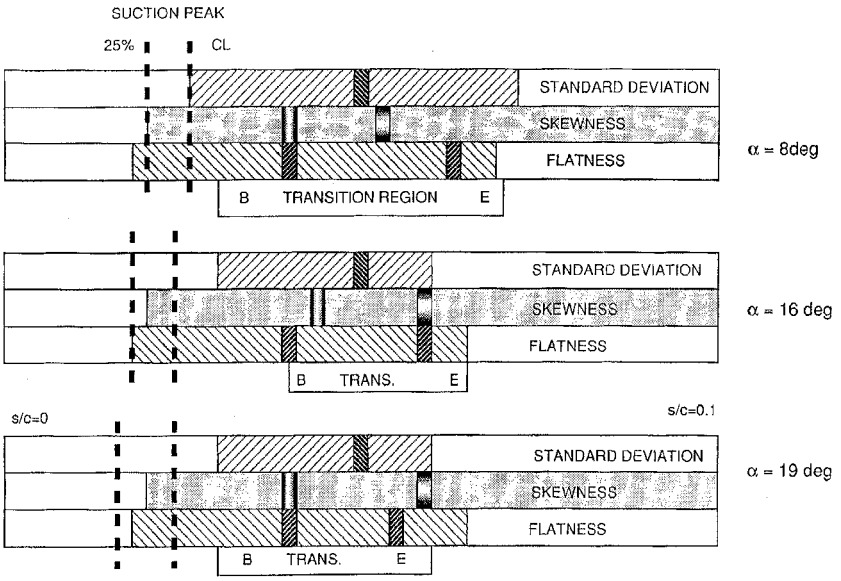

Fig. 1 Experimental transition measurements.

standard deviation of the hot-film signal, which is not completely reliable for high-lift configurations caused by large gradients, does not correlate with any of the normal stresses. Thus, the present situation presents a serious problem to a model that requires selection of a criterion for determining transition onset.

Because of the current situation, we have to resort to an indirect approach for validating the current method. Zero skewness implies an intermittency of $\frac{1}{2}$. Because intermittency is calculated as part of the solution, the location of this value of intermittency is the only way CFD predictions can be compared with hot-film data.

Warren and Hassan[11] showed that a transition onset criterion based on the nonturbulent eddy viscosity correlates well with the minimum skin-friction criterion for flat plates and airfoils. According to this criterion, onset is determined by the requirement

$$R_T = (1/C_\mu)(\nu_{\text{nt}}/\nu) = 1 \tag{11}$$

The need to develop a criterion like this one was a result of the fact that during the transient phase of a CFD computation surface derivatives have a tendency to fluctuate, and the fluctuation can delay or prevent convergence. It was found in Ref. 11 that the expression indicated in Eq. (11) was more forgiving and, in addition, gave accurate results. In the present problem transients are more prevalent. This is evident from the fact that the lift coefficient achieves a steady value long before similar behavior is observed for the drag coefficient.

Addition of Low-Speed Preconditioning

High-lift configurations typically contain regions of very low-speed, separated flow. These tend to degrade the convergence of most Navier–Stokes solvers, making it difficult to conduct a wide array of tradeoff studies in a reasonable amount of time. One means of partially overcoming this convergence degradation is through the use of time-derivative preconditioning.[22–25] Time-derivative preconditioning modifies the eigensystem of the Euler equations such that the wide disparity in characteristic speeds present for low Mach flows is reduced. This can allow uniform convergence rates independent of the Mach number.

As part of this project, the time-derivative preconditioning strategy of Weiss and Smith[25] has been implemented into CFL3D. This involves the development of a Roe-type flux-splitting scheme and a diagonalized alternating-direction implicit time-advancement strategy based on the eigenvalues and eigenvectors of the preconditioned Euler system. The preconditioned Roe interface flux is presented in detail in Appendix A; other details were reported elsewhere.[26] The resulting code, termed CFL3D-P, has been run at Mach numbers as low as 0.0001 without losses in either stability or accuracy. The additions caused by preconditioning scale away as the local Mach number approaches the sonic speed.

Results and Discussion

The results presented here are for the McDonnell Douglas 30P-30N landing configuration for angles of attack α of 19 and 8 deg, freestream Mach number M_∞ of 0.2, and a Reynolds number of 9×10^6. The experimental data[12–15] employed in this study and used to validate the present model were taken in independent wind-tunnel tests. The tunnel used is the Langley Low Turbulence Pressure Tunnel. The turbulent intensity in the tunnel was not measured in any of the preceding experiments. Moreover, there was no attempt to ensure that tests at a given angle of attack were two-dimensional. Further, there was no attempt to assess wall interference effects on α and M_∞. All calculations assume $Tu = 0.05$, as indicated in Ref. 27.

To facilitate comparison with the work of Rumsey et al., the fine grid used in this study is that used in Ref. 2. It is a four-zone free air grid with a freestream extension of about 15 chord lengths. The grid has one-to-one point connectivity in order to ensure conservation across boundaries and provides improved continuity of grid spacing at zonal interfaces. The rigging designation is referred to as 30P-30N. The model has a stowed chord c of 0.5588 m. The ratio of tunnel height to chord is $H/c = 4.09$. The slat and flap settings are for the slat, deflection of 30 deg, gap of 2.95% c, and overhang of -2.5% c; for the flap, deflection of 30 deg, gap of 1.27% c, and overhang of 0.25% c.

In contrast to the work of Ref. 2, it was not possible to obtain a solution using the fully turbulent k–ζ model, as excessive eddy-viscosity growth in the juncture between the slat and the main element prevented adequate convergence. A solution can be obtained if transition is allowed on the slat, and the flow is fully turbulent on the main airfoil and flap. For such a choice the pressure distribution departs from experiment. It is possible to implement the transition/turbulence model by specifying transition onset on all three elements. The resulting pressure distribution, lift, and drag coefficients will depend on the location of selected points.

Because of oscillations in the initial stages of the computations, transition points were initially set. Extensive tests were conducted to ensure that the final results were not dependent on the initial choice of transition points. Moreover, because of lack of computer time, limited tests were conducted to determine when it is safe to switch to the transition criterion indicated in Eq. (11). Switchover can be

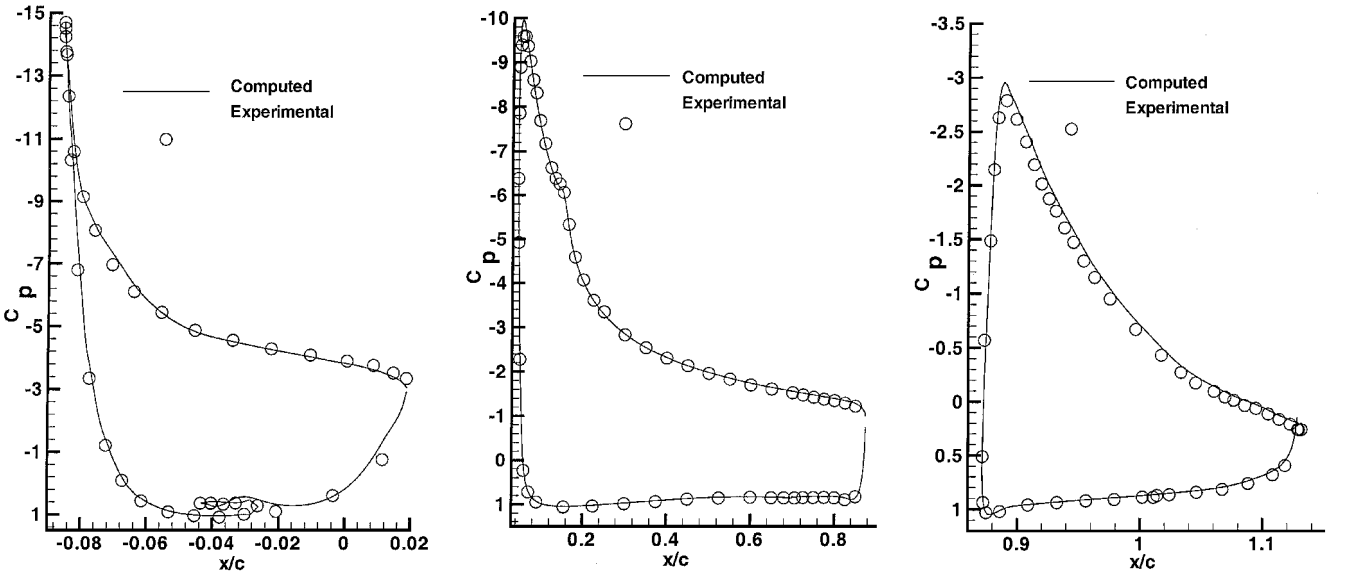

Fig. 2 Pressure distribution for α = 19 deg.

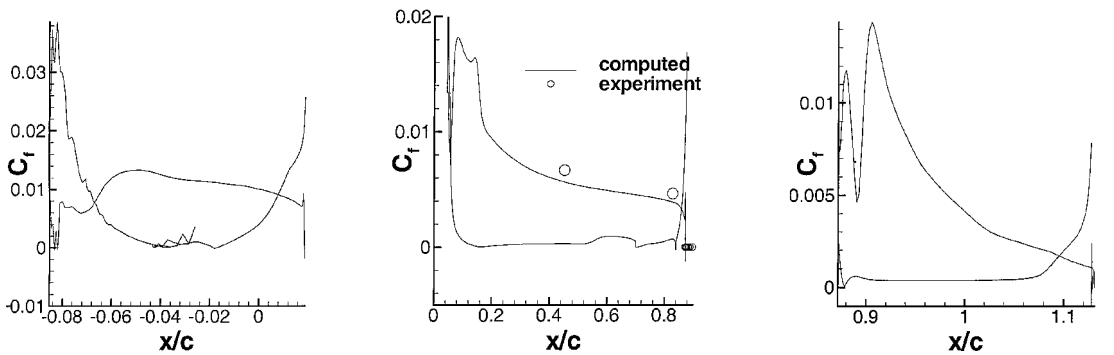

Fig. 3 Skin friction for α = 19 deg.

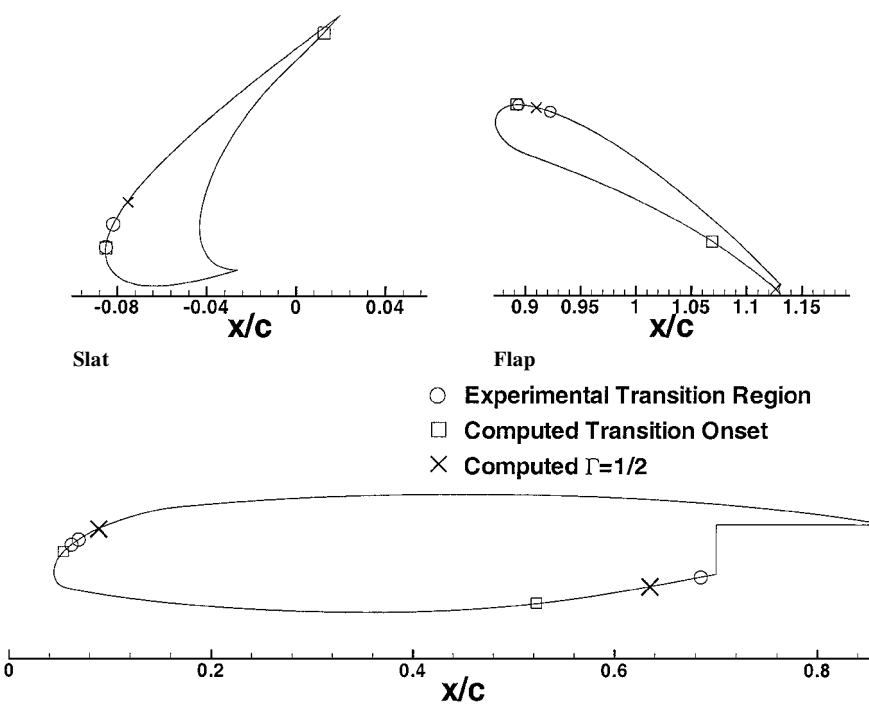

Fig. 4 Comparison of transition points for α = 19 deg.

done when the lift reaches 80–90% of the steady lift appropriate to the selected transition points. Typically, solutions require 3000–4000 iterations to reach steady lift and 5000–6000 iterations to reach steady drag. These numbers are typical of those reported in Refs. 2 and 3.

The first case to be considered is the $\alpha = 19$ deg case. This case was the subject of detailed investigation by Rumsey et al. Figure 2 compares the pressure distribution with experiment. As is seen from the figure, good agreement with experiment is indicated, and the magnitude and location of suction peaks are well predicted on all elements. Figure 3 compares computed skin friction with available experiment.[13] Although data for the slat and flap are not available, good agreement is indicated for available data on the main airfoil.

The predicted transition points are discussed next. Figure 4 compares predictions with experiment. The circles show measured start and end of transition. The squares indicate predicted transition onset, whereas the cross indicates points where the computed $\Gamma = \frac{1}{2}$. Because Γ is an exponential function, the position where predicted transition ends depends on whether $\Gamma = 0.99, 0.995$, etc. Thus, predicted end of transition is not indicated. As shown in Fig. 4, the onset of transition on the upper surfaces of all elements is well predicted. On the slat, calculated $\Gamma = \frac{1}{2}$ is outside the experimentally measured region. Thus, the model is predicting a wider transition region. Moreover, transition is predicted on the lower surface, but the value of Γ remains below 0.5. On the main airfoil $\Gamma = \frac{1}{2}$ is again outside the measured transition region on the upper surface, whereas on the lower surface the transition is predicted early. On the flap $\Gamma = \frac{1}{2}$ is within the experimentally measured region on the upper surface.

Bertelrud[15] adopted the notation of n/a to denote that a definitive start or end of transition was not observed prior to the cusps on the slat and main airfoil or prior to the trailing edge on the flap. Thus, no attempt was made to probe the cove regions for transition. As a result, the predicted transition on the lower surface of the slat and just upstream of the flap trailing edge is not in conflict with the experiment.

The next set of comparisons involve velocity profiles at the six locations indicated in Fig. 5. Figures 6a–6f compare calculated profiles with experiment. Figure 6a compares results at $x/c = 0.1075$. It is indicated in Ref. 2 that the offset velocity difference between computation and experiment is probably a result of improper calibration of experimental data at this station. A number of observations can be made regarding velocity profiles. Although the location and magnitude of the slat wake deficit are not well predicted, its growth rate appears to be well predicted. In general, calculations do an excellent job capturing the main airfoil wake and a fair job capturing the slat wake. Discounting the first station, relative differences between computation and experiment are well within 5%. Two main reasons may be advanced for the observed discrepancies. A slight misalignment in the probe, resulting from the high dynamic pressure in the tunnel, can help explain the differences between computed and

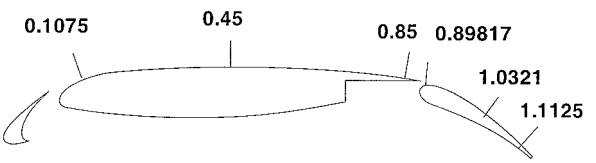

Fig. 5 Locations of *x/c* for velocity profiles.

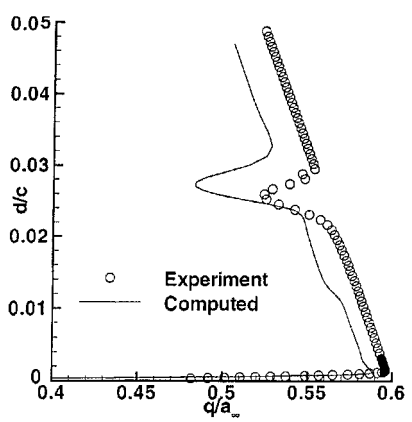

a) *x/c* = 0.1075

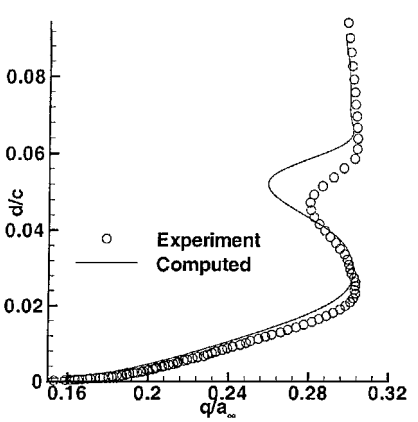

c) *x/c* = 0.85

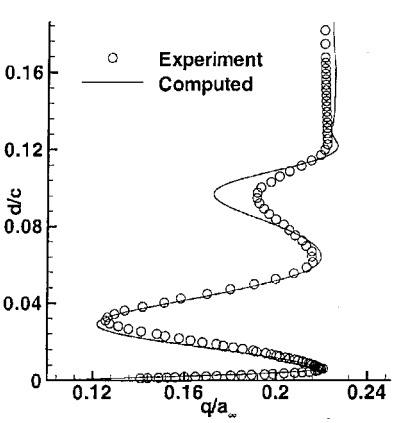

e) *x/c* = 1.0321

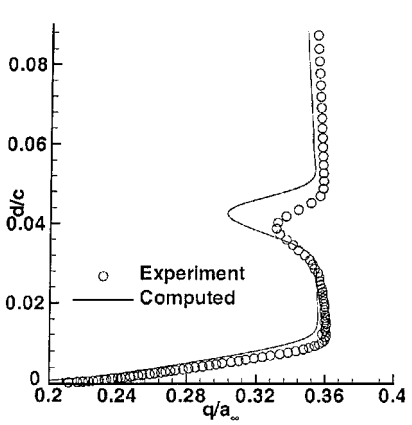

b) *x/c* = 0.45

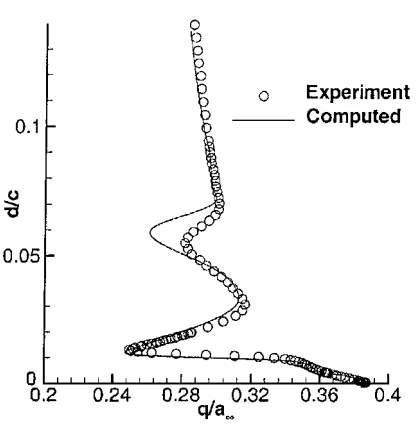

d) *x/c* = 0.89817

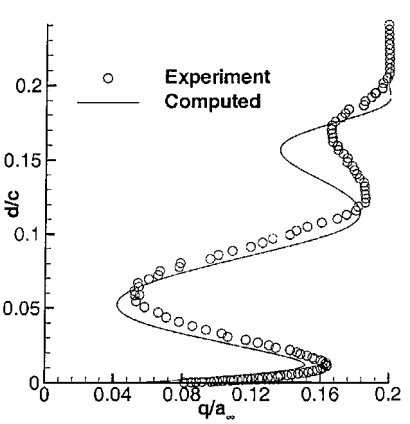

f) *x/c* = 1.1125

Fig. 6 Velocity profiles for α = 19 deg.

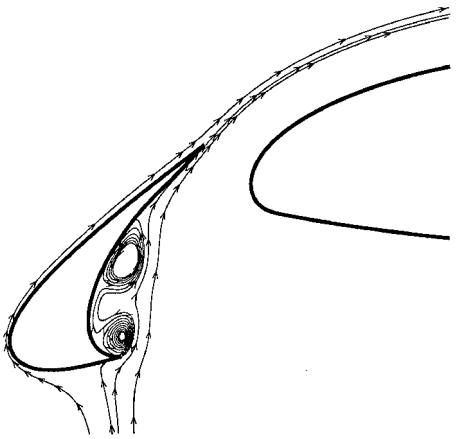

Fig. 7 Slat cove vortices for α = 19 deg.

measured velocities in wake regions. The second is a result of the fact that the flow over the slat is unsteady. Figure 7 shows the existence of two vortices in the cove region. These vortices are never stationary, even when one undertakes a steady calculation. Thus, a time-accurate calculation may be necessary to explain the discrepancy.

The next case to be considered is the $\alpha = 8$ deg case. A third-order-accurate Roe solver was used in generating the results for the $\alpha = 19$ deg case. For the 8-deg case this scheme resulted in an oscillation over the slat, which had no influence over the main airfoil and flap. This was inferred through the movement of the transition point on the upper surface of the slat over 10–12 grid points and is likely caused by the appearance of a laminar separation bubble on the upper surface. The calculations then employed a second-order Roe solver. This stabilized the predicted transition point on the slat, but had no effect on the main airfoil or flap.

Figures 8 and 9 compare the role of the numerical dissipation on the pressure distribution on the slat and vortex structure in the cove region. As is seen from Fig. 8, the pressure distributions in

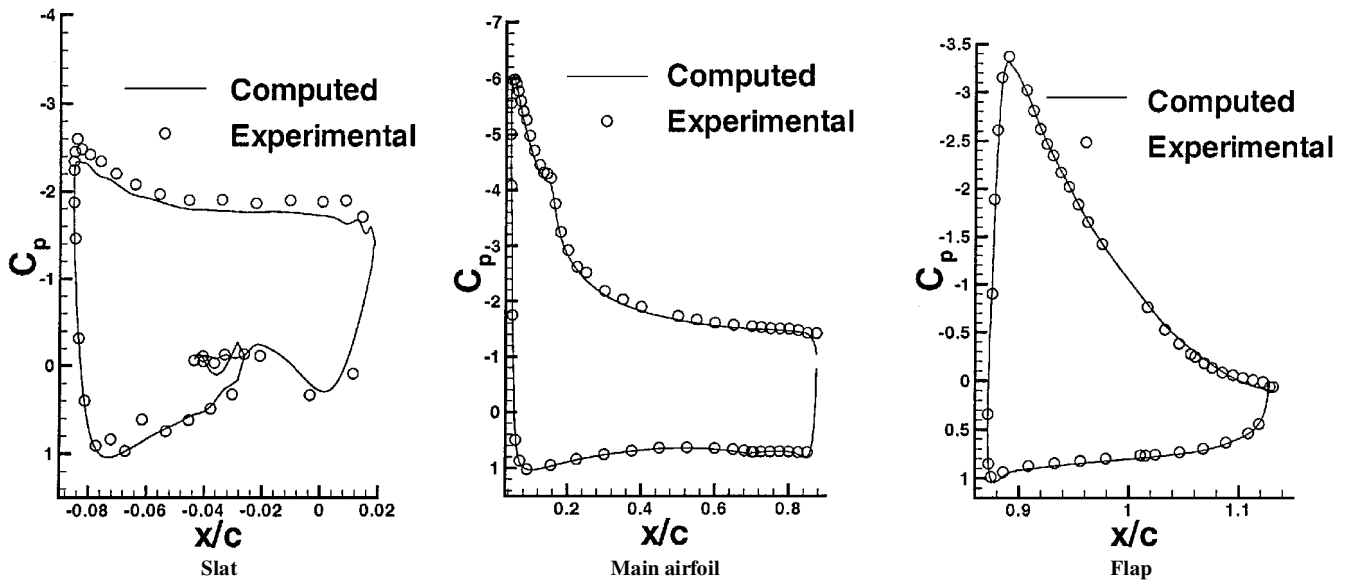

Third-order Roe

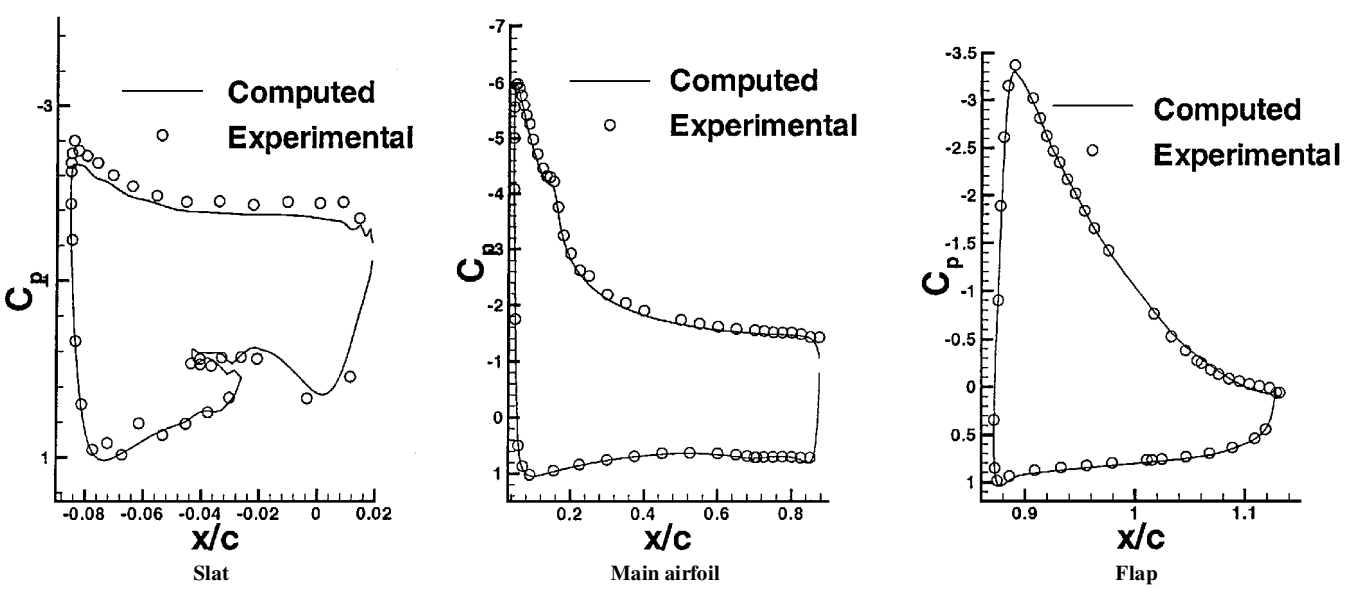

Second-order Roe

Fig. 8 Pressure distribution for α = 8 deg.

the cove region are different, with the second-order results agreeing better with experiment. It is further seen from Fig. 8 that pressure measurements on the slat suggest that the flow is unsteady. Figure 9 shows that the pressure differences in the cove region are a result of the different vortical structures there. The numerical scheme has no influence on the pressure distribution or transition onset on the main airfoil or flap.

Transition prediction for the 8-deg case is discussed next. Unless indicated otherwise, presented results use the second-order Roe solver. As shown in Fig. 10a, the current model predicts delayed transition on the upper surface of the slat, with Γ remaining below $\frac{1}{2}$. Transition is predicted on the lower surface of the slat. As indicated earlier, no attempt was made to probe cove regions. Thus, comparison with experiment for this case is not possible. Figures 10b and 10c indicate that predictions are in good agreement on the main airfoil and flap. Although the model predicts transition on the lower surface of the flap, Γ remains less than $\frac{1}{2}$. Again, as was pointed out earlier, this result is not in conflict with the experiment.

Figure 11 compares velocity profiles. Data are available for the three stations on the main airfoil and the last two stations on the flap. Again discounting the first station, good agreement is indicated, with the maximum relative error on the main airfoil being less than 3%. The penetration of the wake of the main airfoil over the flap is slightly underpredicted. Overall, results indicate that the slat wake is diffuse beyond $x/c = 0.45$, in good agreement with the experiment.

A number of calculations were carried out in which transition onset was assumed. We were unable to find a set of transition points, including those that were suggested by the experiment, that improved upon the velocity profiles, which were generated when the model was allowed to seek transition onset. This suggests that Eq. (11) is a viable criterion for determining transition onset.

Comparison of the $\alpha = 8$ deg results with those of the $\alpha = 19$ deg (see Figs. 2 and 8) reveals that at $\alpha = 8$ deg the main airfoil carries the highest loading, followed by the flap and slat. For $\alpha = 19$ deg, loading on both the main airfoil and slat increases, while loading

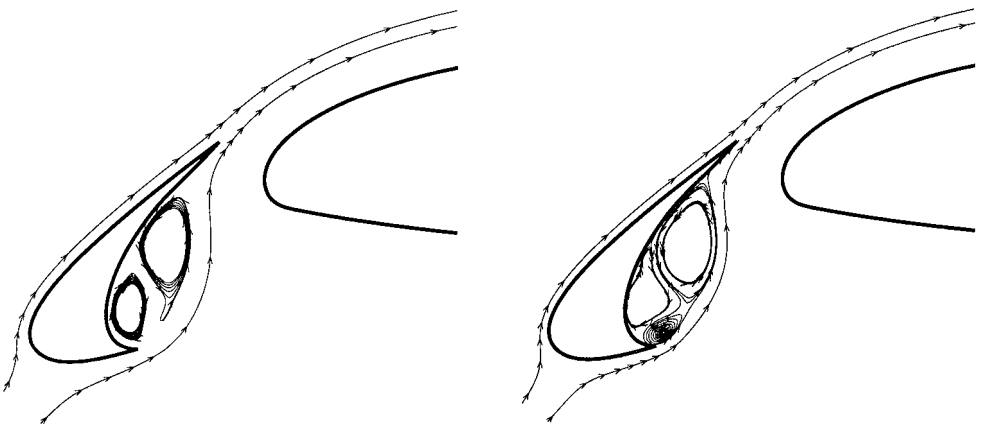

Fig. 9 Slat cove vortices for α = 8.

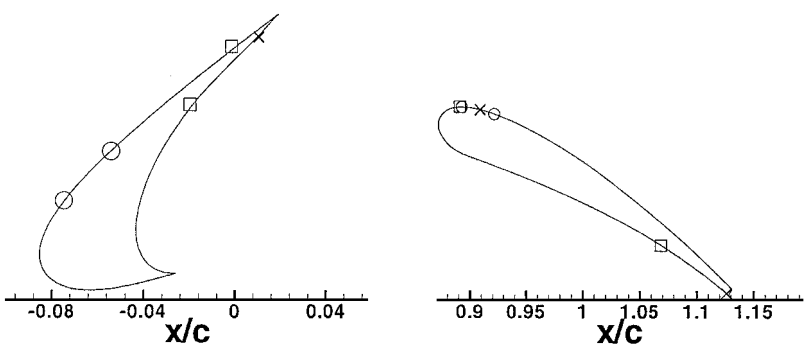

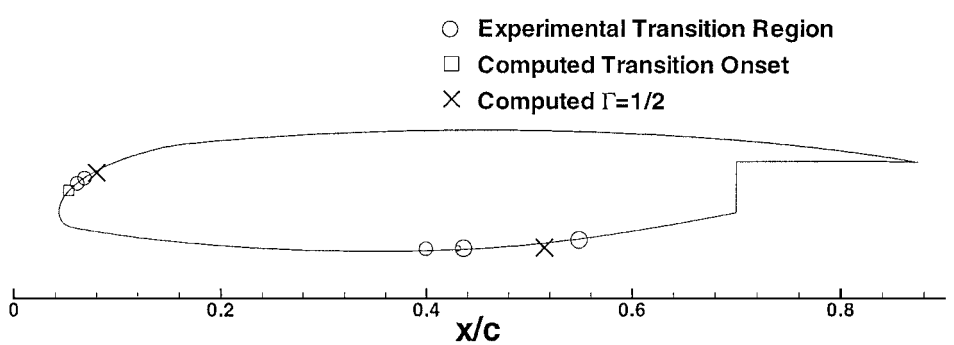

Fig. 10 Comparison of transition points for α = 8 deg.

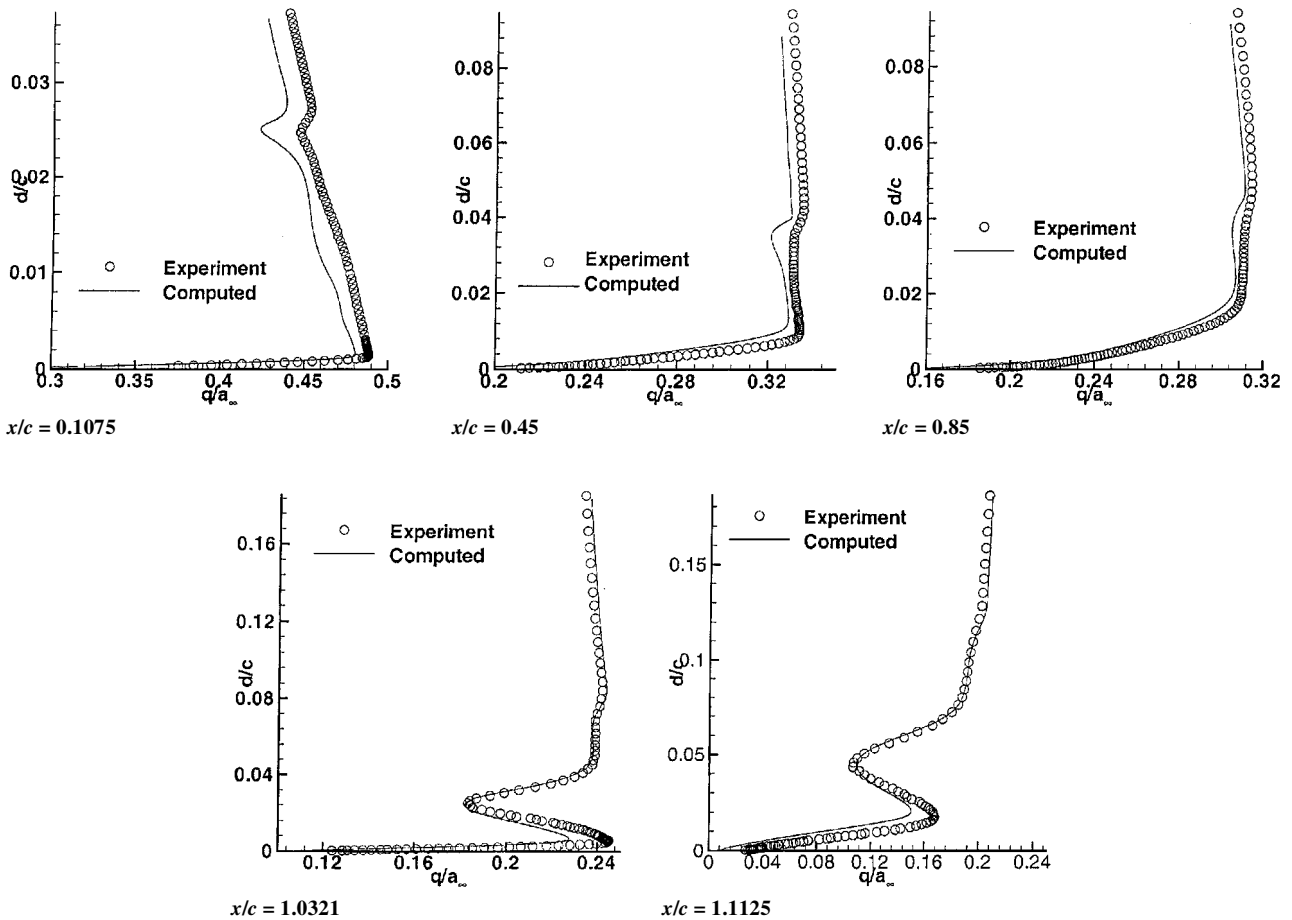

Fig. 11 Velocity profiles for $\alpha = 8$ deg.

on the flap decreases. This behavior is consistent with observations involving three-element airfoils.

Conclusions

The present work represents the first successful attempt to predict transitional/turbulent flow over a multielement airfoil geometry. In general, good agreement is indicated in predicting transition onset and flow velocities. The only disagreement between computation and experiment is in the prediction of the slat wake when $\alpha = 19$ deg: its location and deficit are not well predicted, but its growth rate is. Possible misalignment in the probe and flow unsteadiness in the cove region may account for this discrepancy.

The level of overall agreement suggests that the k–ζ transition/turbulence model captures the essence of the complex flow physics of this problem. This observation, together with earlier successes, suggests that the model can serve as a first step in developing new approaches for studying transition. Further improvements in the model, however, will require well-designed experiments, in which nonintrusive measurements can be used to infer relevant flow parameters and where the condition of the flow environment is well documented.

Appendix: "Preconditioned" Roe Interface Flux

CFL3D-P uses the Weiss–Smith preconditioning matrix,[25] a structurally simple variant of the Turkel/Choi–Merkle family of preconditioners. Given the primitive variable vector $\boldsymbol{V} = [\rho, u, v, w, p]^T$ used by CFL3D-P, the preconditioning matrix G is formed by adding a rank-one matrix to the Jacobian $\partial U / \partial V$:

$$G = \frac{\partial U}{\partial V} + \Theta \boldsymbol{u}\boldsymbol{v}^T \tag{A1}$$

where

$$\boldsymbol{u} = \begin{bmatrix} 1 \\ u \\ v \\ w \\ H \end{bmatrix}, \qquad \boldsymbol{v}^T = [0, 0, 0, 0, 1]^T$$

In this, Θ is defined as

$$\Theta = 1 \Big| \; U_{\text{ref}}^2 - 1/c^2 \tag{A2}$$

where

$$U_{\text{ref}}^2 = \min\left[c^2, \max\left(|\boldsymbol{V}|^2, K|\boldsymbol{V}_\infty|^2\right)\right] \tag{A3}$$

c is the sound speed, $|\boldsymbol{V}|$ is the velocity magnitude, $\boldsymbol{V}_\infty$ is a fixed reference velocity, K is a scaling constant, and H is the total enthalpy per unit mass. Expanded out, the preconditioning matrix takes the following form:

$$G = \begin{bmatrix} 1 & 0 & 0 & 0 & \Theta \\ u & \rho & 0 & 0 & \Theta u \\ v & 0 & \rho & 0 & \Theta v \\ w & 0 & 0 & \rho & \Theta w \\ \frac{1}{2}(u^2 + v^2 + w^2) & \rho u & \rho v & \rho w & 1/(\gamma - 1) + \Theta H \end{bmatrix} \tag{A4}$$

A Roe-type scheme can be derived from the eigenvalues and eigenvectors of the preconditioned equation system. For the ξ coordinate

direction in a computational space, the interface flux may be written as

$$F_{i+\frac{1}{2}} = \tfrac{1}{2}\left[\tilde{F}(V_L) + \tilde{F}(V_R) - \tilde{G}\tilde{T}|\tilde{\Lambda}|\tilde{T}^{-1}(V_R - V_L)\right] \quad \text{(A5)}$$

where $\tilde{T}$ and $\tilde{T}^{-1}$ contain the right and left eigenvectors of the matrix $G^{-1}(\partial E/\partial V)$, $\tilde{\Lambda}$ is the diagonal matrix of eigenvalues, and the tilde notation denotes evaluation at the Roe-average state.

The Roe dissipation vector $\tilde{G}\tilde{T}|\tilde{\Lambda}|\tilde{T}^{-1}(V_R - V_L) \equiv |A_V|(V_R - V_L)$ can be written as

$$|A_V|(V_R - V_L) = \begin{bmatrix} \alpha_4 \\ \tilde{u}\alpha_4 + k_x\alpha_5 + \alpha_6 \\ \tilde{v}\alpha_4 + k_y\alpha_5 + \alpha_7 \\ \tilde{w}\alpha_4 + k_z\alpha_5 + \alpha_8 \\ \tilde{H}\alpha_4 + \tilde{u}\alpha_5 + \tilde{u}\alpha_6 + \tilde{v}\alpha_7 + \tilde{w}\alpha_8 - [\tilde{c}^2/(\gamma - 1)]\alpha_1 \end{bmatrix} \quad \text{(A6)}$$

where

$$\alpha_1 = (|\nabla\xi|/J)|\tilde{\bar{u}}|(\Delta\rho - \Delta p/\tilde{c}^2) \quad \text{(A7)}$$

$$\alpha_2 = (1/2\tilde{c}^2)(|\nabla\xi|/J)|\tilde{\bar{u}}' + \tilde{c}'|(f^+\Delta p + \tilde{\rho}\tilde{c}\Delta\tilde{u}) \quad \text{(A8)}$$

$$\alpha_3 = (1/2\tilde{c}^2)(|\nabla\xi|/J)|\tilde{\bar{u}}' + \tilde{c}'|(f^-\Delta p - \tilde{\rho}\tilde{c}\Delta\tilde{u}) \quad \text{(A9)}$$

$$\alpha_4 = \alpha_1 + \left\{2|\left[M^2_{\text{ref}}(f^+ + f^-)\right]\right\}(\alpha_2 + \alpha_3) \quad \text{(A10)}$$

$$\alpha_5 = [2/(f^+ + f^-)]\tilde{c}(f^-\alpha_2 - f^+\alpha_3) \quad \text{(A11)}$$

$$\alpha_6 = (|\nabla\xi|/J)|\tilde{\bar{u}}|\tilde{\rho}(\Delta u - k_x\Delta\bar{u}) \quad \text{(A12)}$$

$$\alpha_7 = (|\nabla\xi|/J)|\tilde{\bar{u}}|\tilde{\rho}(\Delta v - k_y\Delta\bar{u}) \quad \text{(A13)}$$

$$\alpha_8 = (|\nabla\xi|/J)|\tilde{\bar{u}}|\tilde{\rho}(\Delta w - k_z\Delta\bar{u}) \quad \text{(A14)}$$

The magnitude of the cell interface directed area is $|\nabla\xi|/J$; the direction cosines are

$$k_{x,y,z} = \xi_{x,y,z}/|\nabla\xi| \quad \text{(A15)}$$

and the contravariant velocity normal to the cell interface is denoted as

$$\tilde{u} = k_x u + k_y v + k_z w \quad \text{(A16)}$$

The changes in primitive variables across the cell interface are denoted by

$$\Delta[\,] = [\,]_R - [\,]_L \quad \text{(A17)}$$

and additions caused by preconditioning are defined as follows:

$$\tilde{\bar{u}}' \pm \tilde{c}' = \frac{1}{2}\left[\left(1 + \tilde{M}^2_{\text{ref}}\right)\tilde{\bar{u}} \pm \tilde{c}\sqrt{\left(1 - \tilde{M}^2_{\text{ref}}\right)^2\tilde{M}^2 + 4\tilde{M}^2_{\text{ref}}}\right] \quad \text{(A18)}$$

$$f^+ = \frac{\tilde{\bar{u}}' + \tilde{c}' - \tilde{\bar{u}}}{\tilde{M}^2_{\text{ref}}\tilde{c}} \quad \text{(A19)}$$

$$f^- = -\frac{\tilde{\bar{u}}' - \tilde{c}' - \tilde{\bar{u}}}{\tilde{M}^2_{\text{ref}}\tilde{c}} \quad \text{(A20)}$$

$$\tilde{M}^2 = \frac{\tilde{\bar{u}}^2}{\tilde{c}^2} \quad \text{(A21)}$$

$$\tilde{M}^2_{\text{ref}} = \frac{\tilde{U}^2_{\text{ref}}}{\tilde{c}^2} \quad \text{(A22)}$$

Acknowledgments

This work is supported in part by NASA Grant NAG-1-1991. Part of the computation was carried out at the North Carolina Supercomputing Center and at the National Academy of Sciences. Part of this work was also sponsored by NASA Contract NAS1-97046 while the second author was in residence at the Institute for Computer Applications in Science and Engineering, NASA Langley Research Center, Hampton, Virginia. The authors would like to acknowledge many helpful discussions with N. Chokani of North Carolina State University.

References

[1] Jones, K. M., Biedron, R. T., and Whitlock, M., "Application of a Navier–Stokes Solver to the Analysis of Multielement Airfoils and Wings Using Multizonal Grid Techniques," AIAA Paper 95-1855, June 1995.

[2] Rumsey, C. L., Gatski, T. B., Ying, S. X., and Bertelrud, A., "Prediction of High-Lift Flows Using Turbulent Closure Models," *AIAA Journal*, Vol. 36, No. 5, 1998, pp. 765–774.

[3] Ying, S. X., Spaid, F. W., McGinley, C. B., and Rumsey, C. L., "Investigation of Confluent Boundary Layers in High-Lift Flows," *Journal of Aircraft*, Vol. 36, No. 3, 1999, pp. 550–562.

[4] Reed, H. L., Haynes, T. S., and Saric, W. S., "Computational Fluid Dynamic Validation Issues in Transition Modeling," *AIAA Journal*, Vol. 36, No. 5, 1998, pp. 742–751.

[5] Mateer, G. G., Monson, D. J., and Menter, F. R., "Skin-Friction Measurements and Calculations on a Lifting Airfoil," *AIAA Journal*, Vol. 34, No. 2, 1996, pp. 231–236.

[6] Kusunose, K., and Cao, H. V., "Prediction of Transition Location of a 2-D Navier–Stokes Solver for Multi-Element Airfoil Configurations," AIAA Paper 94-2376, June 1994.

[7] Drela, M., and Giles, B. G., "Viscous-Inviscid Analysis of Transonic and Low Reynolds Number Airfoils," *AIAA Journal*, Vol. 25, No. 10, 1987, pp. 1347–1355.

[8] Wilcox, D. C., *Turbulence Modeling for CFD*, 2nd ed., DCW Industries, Inc., La Cañada, CA, 1998, pp. 137–140.

[9] Bertelrud, A., "Use of Empirical Transition Correlations for Flow Around High-Lift Configurations," AIAA Paper 99-0541, Jan. 1999.

[10] Robinson, D. F., Harris, J. E., and Hassan, H. A., "Unified Turbulence Closure Model for Axisymmetric and Planar Free Shear Flows," *AIAA Journal*, Vol. 33, No. 12, 1995, pp. 2324–2331.

[11] Warren, E. S., and Hassan, H. A., "Transition Closure Model for Predicting Transition Onset," *Journal of Aircraft*, Vol. 35, No. 5, 1998, pp. 769–775.

[12] Spaid, F. W., and Lynch, F. T., "High Reynolds Number Multi-Element Airfoil Flowfield Measurements," AIAA Paper 96-0682, Jan. 1996.

[13] Klansmeyer, S. M., and Lin, J. C., "An Experimental Investigation of Skin Friction on a Multi-Element Airfoil," AIAA Paper 94-1870, June 1994.

[14] Chin, V. D., Peters, D. W., Spaid, F. W., and McGhee, R. J., "Flowfield Measurements About a Multi-Element Airfoil at High Reynolds Numbers," AIAA Paper 93-3137, July 1993.

[15] Bertelrud, A., "Transition on a Three-Element High Lift Configuration at High Reynolds Numbers," AIAA Paper 98-0703, Jan. 1998.

[16] McGinley, C. B., Anders, J. B., and Spaid, F. W., "Measurement of Reynolds Stress Profiles on a High-Lift Airfoil," AIAA Paper 98-2620, June 1998.

[17] Robinson, D. F., and Hassan, H. A., "Further Development of the k–ζ (Enstrophy) Turbulence Closure Model," *AIAA Journal*, Vol. 36, No. 10, 1998, pp. 1825–1833.

[18] Warren, E. S., and Hassan, H. A., "An Alternative to the e^n Method for Determining Onset of Transition," AIAA Paper 97-0825, Jan. 1997.

[19] Dhawan, S., and Narasimha, R., "Some Properties of Boundary Layer Flow During Transition from Laminar to Turbulent Motion," *Journal of Fluid Mechanics*, Vol. 3, No. 4, 1958, pp. 414–436.

[20] Mack, L. M., "Boundary Layer Linear Stability Theory," R-709, AGARD, June 1984, pp. 3.01–3.81.

[21] Walker, G. J., "Transitional Flow on Axial Turbomachine Blading," *AIAA Journal*, Vol. 27, No. 5, 1989, pp. 595–602.

[22] Turkel, E., "Preconditioned Methods for Solving the Incompressible and Low Speed Compressible Equations," *Journal of Computational Physics*, Vol. 72, No. 3, 1987, pp. 277–298.

[23] Choi, Y. H., and Merkle, C. L., "The Application of Preconditioning in Viscous Flows," *Journal of Computational Physics*, Vol. 105, No. 2, 1993, pp. 207–223.

[24] Van Leer, B., Lee, W. T., and Roe, P. L., "Characteristic Time Stepping or Local Preconditioning of the Euler Equations," AIAA Paper 91-1552, July 1991.

[25] Weiss, J. M., and Smith, W. A., "Preconditioning Applied to Variable and Constant Density Time-Accurate Flows on Unstructured Meshes," AIAA Paper 94-2209, June 1994.

[26] Edwards, J. R., and Thomas, J. L., "Development of $\mathcal{O}(Nm^2)$ Preconditioned Multigrid Solvers for Euler and Navier–Stokes Equations," *AIAA Journal*, Vol. 38, No. 4, 2000, pp. 717–720.

[27] Wleizen, R. W., Spencer, S. A., and Grubb, J. P., "Comparison of Flow Quality in Subsonic Pressure Tunnels," AIAA Paper 94-2503, June 1994.